

Muonium formation via electron transport in solid nitrogen

V. Storchak

Russian Research Centre "Kurchatov Institute," Kurchatov Square 1, Moscow 123182, Russia

J. H. Brewer, G. D. Morris, D. J. Arseneau, and M. Senba*

Canadian Institute for Advanced Research and Department of Physics and Astronomy, University of British Columbia, Vancouver, British Columbia, Canada V6T 1Z1

(Received 2 July 1998)

Muon spin rotation (μ SR) techniques have been used to investigate the diamagnetic and paramagnetic states of energetic positive muons stopped in solid molecular nitrogen. The paramagnetic signal arises from muonium ($\text{Mu} = \mu^+ + e^-$) atoms and reflects both "prompt" epithermal Mu formation and "delayed" thermal Mu formation. The latter is shown to be due to convergence of the thermalized μ^+ with an electron liberated in its ionization track. Measurements in external electric fields of up to 10 kV/cm applied along and antiparallel to the initial muon momentum reveal a large anisotropy in the spatial distribution of muon-electron pairs: the μ^+ is shown to thermalize "downstream" of the ionization products of its track. The characteristic muon-electron distances in α -N₂ and β -N₂ and liquid nitrogen are estimated to be approximately 500 Å, 250 Å, and 300 Å, respectively. The dependence of delayed Mu formation upon electron mobility offers a method for determining such mobilities on a microscopic scale. Electron drift mobilities are shown to differ by several orders of magnitude in the α and β phases of solid nitrogen. Excess electrons from the muon track are apparently delocalized in orientationally ordered α -N₂; electron localization in orientationally disordered β -N₂ is discussed in terms of the formation of a small polaron due to electron interaction with the rotational degrees of freedom of N₂ molecules. The diamagnetic signal in condensed nitrogen is ascribed to the N₂ μ^+ molecular ion; in β -N₂ it consists of two components, one relaxing slowly due to random fields from nuclear dipole moments and the other relaxing up to two orders of magnitude faster, due to *very* delayed Mu formation as the muon captures low-mobility electrons. [S0163-1829(99)10815-4]

I. INTRODUCTION

Ever since the discovery¹ in 1957 of parity nonconservation in $\pi \rightarrow \mu \rightarrow e$ decay, beams of polarized positive muons (μ^+) have been used to probe materials. (For an early review see, e.g., Ref. 2.) In the past several decades the techniques of muon spin rotation/relaxation/resonance³ (μ SR) have been developed into a powerful tool providing valuable information regarding various chemical and solid-state physics phenomena. Studying materials using μ SR has to date involved irradiation of the samples under investigation with positive muons of several MeV initial kinetic energy. The time evolution of the muon spin polarization is then monitored on the time scale of the muon lifetime (2.197×10^{-6} s) by means of the muon's asymmetric decay; the resultant time spectra allow one to distinguish between signals arising from muons in diamagnetic environments and those from muons in paramagnetic states such as muonium ($\text{Mu} = \mu^+ + e^-$) atoms⁴ or "muonated" free radicals.⁵ Although the final chemical state of the incoming μ^+ has long been recognized to depend critically upon the medium under study, there is still no self-consistent theory that can reliably predict the initial distribution of the muon polarization between diamagnetic and paramagnetic states or their possible interconversions.

The situation is best understood in the *gaseous* phase, where the initial formation and subsequent reaction of paramagnetic and diamagnetic species have been studied intensively for many years.⁶⁻⁸ The situation in the *condensed*

phases seems to be much more complicated. In particular, our understanding of Mu formation in *solids* is rather fragmentary and controversial, despite the widespread use^{9,10} of the μ^+ and muonium as probes of superconductors and superfluids, metals and magnets, semiconductors and insulators, etc. Although many such experiments rely on the muon only to obtain information about its ultimate magnetic environment, in other cases it is extremely important to understand the mechanisms of formation of different muon states in order to correctly interpret the experimental data.

Although the μ^+ is almost an order of magnitude lighter than the proton, it is so much heavier than the electron that the Mu reduced mass is almost the same as that of the hydrogen atom. The Born-Oppenheimer approximation is therefore valid, giving Mu almost the same ionization potential (13.54 eV) and electronic structure as the H atom. For this reason muonium may properly be considered a light hydrogen isotope; as such, Mu is expected to exhibit chemical and condensed-matter states analogous to those of H. This image has provoked extensive studies of various phenomena that complement our prior knowledge of the states and dynamics of simple atoms in matter. In particular, studies of Mu dynamics in insulators and semiconductors have revealed different mechanisms of quantum tunneling phenomena¹¹ that are much less pronounced for the heavier hydrogen atom. Investigations of semiconductors^{12,13,10} led to the discovery of Mu states in these materials, the analogous hydrogen atom states of which were previously unknown. Slow relaxation of the muon polarization in certain

magnetic insulators^{14,15} has recently been interpreted in terms of exotic magnetic properties of the host lattice. Such important studies are hampered by our inadequate knowledge of Mu formation mechanisms in solids and may even be subject to erroneous interpretation in some cases if delayed Mu formation mimics the phenomena under study.

Muonium formation in low-pressure gases has been explained¹⁶ by analogy with hydrogen atom formation under proton irradiation involving the well-known phenomenon of *charge exchange*.¹⁷ Muonium atoms formed this way are usually referred to as “prompt” Mu. For high-energy muons (down to about 10 keV), Bethe-Bloch ionization dominates; at lower μ^+ energies cyclic charge exchange takes over until the muon thermalizes. In the elementary charge exchange cycle the muon picks up an electron directly from an atom or molecule of the medium to form a neutral Mu atom and then loses it to become a positive ion again. (The negative Mu^- ion is also formed occasionally¹⁸ but is quickly stripped of its extra electron.) The relative likelihood of electron pickup and loss is determined by their respective cross sections at a given energy. In this model, if the muon slows to less than a certain energy ε_c^+ as a positive ion, it can no longer capture an electron and will thermalize as a μ^+ ; conversely, if it drops below some other energy ε_c^0 as a neutral atom, it can no longer lose its electron and will thermalize as a Mu atom. The “history” of the charge exchange cycle is important in low-pressure gases inasmuch as the muon polarization begins to evolve *via* the hyperfine interaction each time Mu is formed; after many cycles these small changes may add up to a measurable depolarization.¹⁹ In condensed matter the time scale is too short for this mechanism to be important.

One might expect the ionization potential ε_I of the medium to provide a qualitative criterion for Mu formation: if ε_I is higher than the Mu binding energy ($\varepsilon_{\text{Mu}} = 13.54$ eV) the yield of thermalized muonium may be expected to be low, whereas in a substance with $\varepsilon_I < \varepsilon_{\text{Mu}}$ one would expect most muons to form Mu atoms. However, one *cannot* simply associate ε_c^+ with $\varepsilon_I - \varepsilon_{\text{Mu}}$ and ε_c^0 with $\varepsilon_{\text{Mu}} - \varepsilon_I$. The dominant final state tends to be determined by the respective cross sections at higher energies than either ε_I or ε_{Mu} , even in gases.²⁰

This simplified picture of isolated inelastic collisions may be a reasonable model for Mu formation processes in *gases*, but in *solids* one must confront a complicated picture of many-body collisions and collective phenomena. For Mu formation in condensed media, any simple criterion based on ionization potentials leads to conclusions that contradict the experimental data. For example, in solid hydrogen ($\varepsilon_I = 15.43$ eV) approximately 15% of stopping muons form muonium.²¹ In an even more extreme case, a large Mu fraction was observed²² in superfluid ^4He despite the fact that the ionization potential of the helium atom ($\varepsilon_I \approx 25$ eV) considerably exceeds that of Mu. A large Mu fraction (approximately 80%) was found in solid neon,²³ where $\varepsilon_I \approx 22$ eV. In liquid neon the Mu formation probability was measured to be approximately 20%.²³ In both superfluid He and solid Ne, Mu formation processes were found to be temperature dependent. This circumstance is hard to explain in terms of “prompt” muonium formation at energies far above thermal. Solid nitrogen ($\varepsilon_I = 15.6$ eV) even exhibits a *nonmonotonic* temperature dependence of the diamagnetic²⁴ and Mu^{25}

fractions, having peculiarities at the α - β transition. The diamagnetic fraction also shows a strong temperature dependence²⁶ in solid CO ($\varepsilon_I = 14.01$ eV), which could be considered a close analogue of solid nitrogen,²⁷ with similar but smaller peculiarities at the α - β transition temperature.²⁸ All these examples show that in saturated systems where the muon polarization is believed to be distributed between only two muon states — diamagnetic and muonium — Mu is formed even if $\varepsilon_I > \varepsilon_{\text{Mu}}$. On the other hand, in solid natural xenon²⁹ and isotopically pure ^{136}Xe ,²⁸ experiments reveal a noticeable diamagnetic fraction despite the fact that their ionization potential (12.13 eV) is much lower than that of the Mu atom. Obviously, in condensed matter the mechanisms of muonium formation must include other processes besides “prompt” epithermal Mu formation.

It is important to distinguish between the qualitative model of epithermal Mu *formation* described above and the so-called “hot atom” model^{30,31,6,20} of the *chemical reactions* of Mu, in which the placement of the μ^+ in stable diamagnetic molecules is accomplished during the slowing down process when either the μ^+ or the neutral Mu atom has enough kinetic energy (a few eV) to engage in endothermic chemical reactions that are inaccessible to it at thermal energies. That such reactions are possible is undeniable, but their importance relative to interactions between Mu (or the μ^+) and the radiolysis products of its ionization track has been a perennial topic of debate. In the so-called “spur model”,^{32–34} the differentiation of the incoming muons into various charge states takes place at thermal energies after the muon (or Mu atom) has come to rest in the medium. Interconversion between such states can be an ongoing process, terminated only when the radiolysis species (free electrons or reactive ions) produced at or near the end of the muon ionization track (or “spur”) have dissipated or recombined in “geminate” processes.⁶ Since the convergence of a radiolysis electron with the μ^+ to form muonium takes some time, Mu atoms formed this way are often referred to as “delayed” Mu to be distinguished from “prompt” Mu formed at epithermal energies. However, these two Mu formation processes are often indistinguishable experimentally, as both of them may take place at times shorter than can be resolved directly by ordinary μSR techniques.³ In principle, formation times can be estimated indirectly by measuring the effect of varying external magnetic field on the time evolution of the muon polarization as in the presence of fast chemical reactions.^{30,31,35–37} Inasmuch as the “spur model” takes into account interactions of the thermalized muon with products of its ionization track, the present work might be taken as confirmation of its validity; however, since we are not concerned here with diamagnetic molecular products of chemical reactions of μ^+ or Mu, our results do not address the question of whether “hot atom” reactions play a role comparable to that of “spur” reactions in the chemistry of muons and muonium.

In *cryocrystals* and *cryoliquids* (substances that are gaseous at room temperature and atmospheric pressure) the μ^+ often thermalizes far enough from the last free electrons liberated in its ionization track that its Coulomb attraction for them can be overcome by an externally applied electric field. The effect of electric fields on delayed Mu formation was first observed in superfluid ^4He ;²² similar effects in solids

were first observed²⁵ in the α phase of solid nitrogen ($s\text{-N}_2$). In both cases, Mu formation was quenched by application of an electric field in the same direction as the initial muon momentum (denoted $E > 0$); however, in $\alpha\text{-N}_2$ Mu formation was *enhanced* by an electric field in the opposite direction ($E < 0$), whereas in superfluid ^4He a negative E again decreased the Mu formation probability — albeit less strongly than a positive E of equal magnitude. This indicates a strong anisotropy in the spatial distribution of muon-electron pairs in both $\alpha\text{-N}_2$ and superfluid ^4He .

Another advantage of cryocrystals and cryoliquids is that free carriers in these media have tremendous differences in *mobility*, ranging from delocalized free electrons to *polarons* (quasiparticles composed of, e.g., electrons and the lattice distortion they produce — and carry around with them) with huge effective masses and extremely low mobilities. In some cases both types may be present simultaneously. As a result, delayed Mu formation may take place so rapidly as to be complete long before the observable time window of any μSR experiment (a few ns to 10–20 μs); or it may occur over many microseconds and be clearly visible through its depolarizing effect on the diamagnetic μ^+ precession signal. This offers an opportunity to study delayed Mu formation directly in “real time.” It is also a source of concern for those who study “ordinary” insulators with μSR , since delayed Mu formation *via* low-mobility carriers can mimic other forms of relaxation that are the object of their investigations. Direct evidence has been seen for *very* delayed Mu formation in liquid ^3He ,³⁸ liquid neon,^{39,40} and other rare-gas liquids and solids,⁴¹ as well as in solid nitrogen^{25,42} and sapphire.⁴³

In solid nitrogen a strong correlation was found between the Mu formation probability and the electron mobility b_e , especially around the $\alpha\text{-}\beta$ transition temperature $T_{\alpha\beta}$ between the low-temperature orientationally ordered α phase and the high-temperature β phase. Further experiments⁴² revealed that b_e in $\alpha\text{-N}_2$ is approximately five 5 orders of magnitude higher than that in $\beta\text{-N}_2$.

The present paper reports a detailed study of muonium atom formation in solid nitrogen throughout the temperature range 10–64 K in various magnetic and electric fields. Experiments show that in both $\alpha\text{-N}_2$ and $\beta\text{-N}_2$ the muonium fraction is at least partially due to “delayed” Mu formed by transport of radiolysis electrons to thermalized muons. Electron transport mechanisms in the different solid phases of nitrogen and their dependence on the orientational ordering of N_2 molecules are discussed in detail.

II. EXPERIMENTAL ASPECTS AND DATA ANALYSIS

The experimental technique used in these measurements, positive muon spin rotation/relaxation, has been described in considerable detail in a number of review articles and books;^{2,3,6} we therefore present here only those features of special relevance to this experiment. Spin-polarized surface muons (momentum ≈ 28 MeV/ c) from the M13, M15, or M20 beam line at TRIUMF were stopped in solid nitrogen samples inside a cold-finger cryostat at the center of a μSR spectrometer. A magnetic field was applied perpendicular to the initial muon spin polarization. Under these conditions two possible types of muon states — diamagnetic (usually a

molecule or molecular ion) and paramagnetic (usually a muonium atom) — could be easily distinguished by their respective Larmor frequencies: in a weak (~ 1 mT) transverse magnetic field H , those muons which form Mu precess at a characteristic triplet Larmor frequency $\omega_{\text{Mu}} \approx -103 \omega_\mu$, where $\omega_\mu = \gamma_\mu H$ is the Larmor frequency of a muon in a diamagnetic environment and $\gamma_\mu = 2\pi \times 135.5$ MHz/T is the muon gyromagnetic ratio. [Triplet muonium precesses in the opposite *sense* to the μ^+ , having essentially the electron’s magnetic moment; hence the $-$ sign.] Regardless of its chemical environment, the muon decays with a constant probability per unit time τ_μ^{-1} (where $\tau_\mu = 2.176 \times 10^{-6}$ s is the mean muon lifetime); a positron (e^+) emitted in $\mu^+ \rightarrow e^+ + \nu_e + \bar{\nu}_\mu$ decay exits preferentially along the muon spin direction at that instant. Two pairs of plastic scintillation e^+ counters (“back-front” and “up-down”) surrounded the cryostat tail except for a small hole where the muon beam entered, passing through a thin μ^+ counter. Time-differential μSR electronics accepted only those events in which each outgoing positron could be unambiguously associated with one incoming muon. For each implanted muon the individual decay time t was measured and the corresponding bin was incremented in the time histogram associated with the detector in which the e^+ was detected. As a result, the accumulated positron time histograms directly reflect the time evolution of the muon spin polarization. The numbers of events collected at decay time t in each counter of a pair (e.g., N_F and N_B) are given by

$$N_F(t) = b_F + N_F^0 e^{-t/\tau_\mu} [1 + A_F^0 \hat{n}_F \cdot \vec{P}_\mu(t)],$$

$$N_B(t) = b_B + N_B^0 e^{-t/\tau_\mu} [1 + A_B^0 \hat{n}_B \cdot \vec{P}_\mu(t)], \quad (1)$$

where F and B stand for the “forward” and “backward” positron counters (relative to the muon beam direction). [Analogous formulas hold for the “up” (U) and “down” (D) histograms.] Here b_F and b_B are time-independent backgrounds (usually determined from $t < 0$ bins and removed numerically as shown below), N_F^0 and N_B^0 are normalization factors, A_F^0 and A_B^0 are empirical maximum muon decay asymmetries (usually ≈ 0.2 to 0.3) and the term on the right is the projection of the muon spin polarization $\vec{P}_\mu(t)$ onto the effective symmetry axis of the corresponding detector. The experimental setup is usually designed so that $\hat{n}_B \approx -\hat{n}_F \approx \hat{z}$, in which case one can approximate $P_z(t)$, the z component of the muon polarization, in terms of the so-called “corrected asymmetry”

$$A_B^0 P_z(t) = \frac{(\alpha_{BF} - 1) + (\alpha_{BF} + 1) a_{BF}(t)}{(\alpha_{BF} \beta_{BF} + 1) + (\alpha_{BF} \beta_{BF} - 1) a_{BF}(t)}, \quad (2)$$

where

$$a_{BF}(t) \equiv \frac{[N_B(t) - b_B] - [N_F(t) - b_F]}{[N_B(t) - b_B] + [N_F(t) - b_F]} \quad (3)$$

is the so-called “raw asymmetry” and

$$\alpha_{BF} \equiv \frac{N_F^0 - b_F}{N_B^0 - b_B} \quad \text{and} \quad \beta_{BF} \equiv \frac{A_F^0}{A_B^0} \quad (4)$$

are relatively uninteresting empirical systematic parameters (as is A_B^0) to be determined by fitting calibration spectra. Usually $\beta_{BF} \approx 1$, in which case Eq. (2) reduces to

$$A_B^0 P_z(t) \approx \frac{\left(\frac{\alpha_{BF} - 1}{\alpha_{BF} + 1} \right) + a_{BF}(t)}{1 + \left(\frac{\alpha_{BF} - 1}{\alpha_{BF} + 1} \right) a_{BF}(t)},$$

which approaches $a_{BF}(t)$ in the limit of $\alpha_{BF} \rightarrow 1$. Thus the time evolution of each component of the muon spin polarization can be determined from the corresponding pair of positron histograms.

In transverse magnetic field the overall ‘‘signal’’ (corrected asymmetry) presents an oscillating pattern of the form

$$A_B^0 P_z(t) = A_{\text{Mu}} G_{xx}^{\text{Mu}}(t) \cos(\omega_{\text{Mu}} t + \phi_{\text{Mu}}) + A_{\text{D}} G_{xx}^{\text{D}}(t) \cos(\omega_{\text{D}} t + \phi_{\text{D}}), \quad (5)$$

where A_{Mu} , A_{D} , ϕ_{Mu} , and ϕ_{D} are the amplitudes and initial phases of the muonium and diamagnetic signals, respectively. (Recall that $\omega_{\text{Mu}} = -102.88 \omega_{\mu}$; these parameters are not really independent.) The relaxation functions $G_{xx}^{\text{Mu}}(t)$ and $G_{xx}^{\text{D}}(t)$ for Mu and μ^+ signals describe the decay of the amplitude of the corresponding component; this ongoing depolarization may have many causes, from random static local fields due to nearby nuclear moments (which usually produce a Gaussian decay envelope) to fluctuating nuclear hyperfine couplings or chemical reactions (which usually produce an exponential decay). We shall be concerned mainly with the latter variety, for which the relaxation can be characterized by a simple exponential relaxation rate:

$$G_{xx}^{\text{Mu}}(t) = e^{-\lambda_{\text{Mu}} t} \quad \text{and} \quad G_{xx}^{\text{D}}(t) = e^{-\lambda_{\text{D}} t}, \quad (6)$$

where $T_2^{\text{Mu}} = \lambda_{\text{Mu}}^{-1}$ and $T_2^{\text{D}} = \lambda_{\text{D}}^{-1}$ are the ‘‘transverse relaxation times’’ of the Mu and diamagnetic components, analogous to the free induction decay time in NMR after a 90° pulse for a spin- $\frac{1}{2}$ nucleus.

Typical asymmetry spectra in solid nitrogen at $T = 29$ K are shown in Fig. 1 for magnetic fields of 0.65 mT (a) and 6.5 mT (b). Note the different time scales for these two spectra. The solid line in Fig. 1(a) is a minimum- χ^2 fit of the experimental data to Eqs. (5) and (6). The solid line in Fig. 1(b) is a fit without the muonium signal, which is eliminated by adjusting the time bin width to a large integer multiple of the Mu precession period. The diamagnetic amplitude A_{D} was measured at low and at high magnetic fields and was determined to be essentially field independent. The muonium amplitude A_{Mu} was determined at low fields; its magnetic field dependences at different temperatures are discussed in detail below.

Only ultrahigh-purity nitrogen gas (impurity content $\leq 10^{-5}$) from several different cylinders was used in the experiment. Special attention was paid to control of paramagnetic impurities, in particular oxygen. The whole system for sample preparation, including the sample cell inside the cryostat, the gas handling system, electrical connections, etc., was pumped down to a pressure on the order of 10^{-6} torr for several days before the experiments. There was

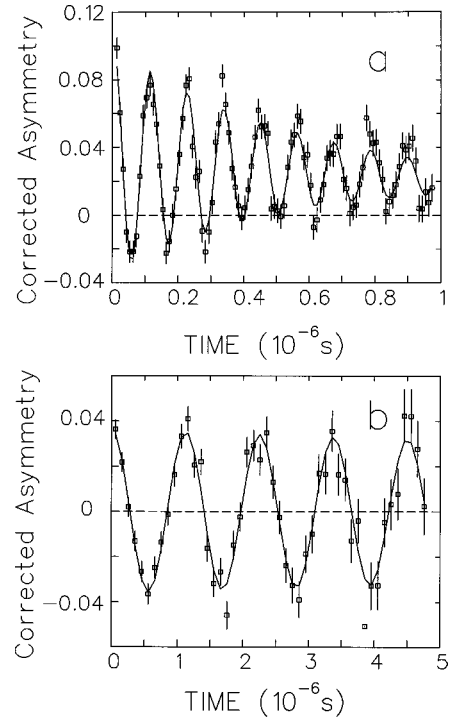


FIG. 1. (a) μ SR precession spectrum in s - N_2 in a transverse magnetic field of 0.65 mT. (b) Diamagnetic precession signal in s - N_2 in a transverse magnetic field of 6.5 mT. The muonium signal is averaged to zero by adjusting the binning width to a large integer multiple of the Mu precession period. Note the different time scales in (a) and (b).

found to be no noticeable difference between sets of results obtained with nitrogen from different cylinders or on different muon beamlines.

Gaseous nitrogen was liquidized directly from the gas cylinder or from a 5-L glass bulb into a square copper sample cell 22 mm on a side and 6 mm thick attached to the cold finger of the cryostat. The front and back of the cell were sealed with 0.125-mm-thick transparent Mylar windows. The vacuum jacket of the cryostat tail also had transparent Mylar windows which allowed us to inspect nitrogen condensation and crystal growth. Solid nitrogen crystals were grown at an average speed of about 4 mm/h in a temperature gradient of up to 5 K over the sample, warmest at the top. Only perfectly transparent crystals without any visible defects were used in the experiments.

The muon beam was usually collimated down to a diameter of 9–12 mm, centered on the cell window. The fraction of muons stopped in the Mylar windows was estimated to be less than 10%; therefore essentially all the muons were stopped in the nitrogen sample.

Temperature control was carried out by means of two calibrated thermometers: a Si diode on the cold finger of the cryostat and a $\text{Al}_{1-x}\text{Ga}_x\text{As}$ thermometer in the sample cell. The accuracy of the sample temperature measurements was not worse than ± 0.1 K.

An external electric field of up to 10 kV/cm was generated by means of two parallel grids of very fine wires located on the front and back of the sample cell. The distance between the grids was 12 mm. Electric field polarity was easily changed between positive (parallel to the initial muon mo-

mentum) and negative (opposite to the initial muon momentum) by changing the high-voltage polarity applied to the grids. The inhomogeneity of the electric field in the central part of the sample (experimental volume) was estimated to be approximately $\pm 2\%$.

III. ORIENTATIONAL TRANSITION IN SOLID NITROGEN

Solid nitrogen under its own vapor pressure crystallizes in two solid phases. The low-temperature α -N₂ phase is face-centered cubic²⁷ for temperatures up to $T_{\alpha\beta}=35.6$ K. The β -N₂ phase has a stable hexagonal close-packed crystal structure at higher temperatures up to the melting point $T_m=63.14$ K.²⁷ It is established that the equilibrium molecular configuration and the nature of molecular motions in these two phases are both determined by an electric quadrupole-quadrupole interaction between the molecules.^{44,45} In a unit cell of α -N₂ the diatomic molecules (whose centers of mass are at the lattice sites) are frozen along four different equilibrium directions along the diagonals of the cube, but undergo small-angle librations around these directions. The phase transition in solid nitrogen has long been known to be accompanied by a drastic change in molecular orientational motion.^{27,46} The β -N₂ phase is known to be orientationally disordered, although the centers of mass of the N₂ molecules are still at the lattice sites. X-ray diffraction studies of β -N₂ (Ref. 47) are equally consistent with either a coherent hindered rotation of N₂ molecules or statistically disordered individual molecular precession. Either model indicates that in the β -phase the molecules all maintain an angle close to the ‘‘magic’’ angle of $54^\circ 44'$ between their long axes and the \hat{c} axis of the crystal, which averages to zero the electric-field gradient of the molecular field.

The theory of orientational ordering in solid nitrogen^{27,48,49} determines the dominant role of the processes in the librational crystal subsystem while the hcp-bcc transition is treated as a secondary phenomenon in the α - β transition. Independent of the particular model of the β phase, that theory determines the α - β transformation in solid nitrogen to be a *first-order* phase transition accompanied by a large jump in the orientational order parameter, and therefore a typical *order-disorder* transition.

Many peculiarities of the dynamical properties of solid nitrogen (as well as other simple heteroatomic solids) are connected with the rotational motion of molecules. In particular, the rotational motion of molecules determines to a certain extent the thermodynamic, kinetic, and spectroscopic properties of s -N₂.²⁷ At first glance it may seem hard to establish any connection between muonium atom formation and the rotational dynamics of molecules. Nevertheless, in this paper we will demonstrate a direct influence of the orientational motion of nitrogen molecules on the Mu formation phenomenon in solid nitrogen.

IV. EXPERIMENTAL RESULTS AND DISCUSSION

Both muonium and diamagnetic fractions were observed in solid nitrogen at all temperatures. It was found that the diamagnetic signal itself clearly has both a slow-relaxing (*S*) and a fast-relaxing (*F*) component in β -N₂ and around the

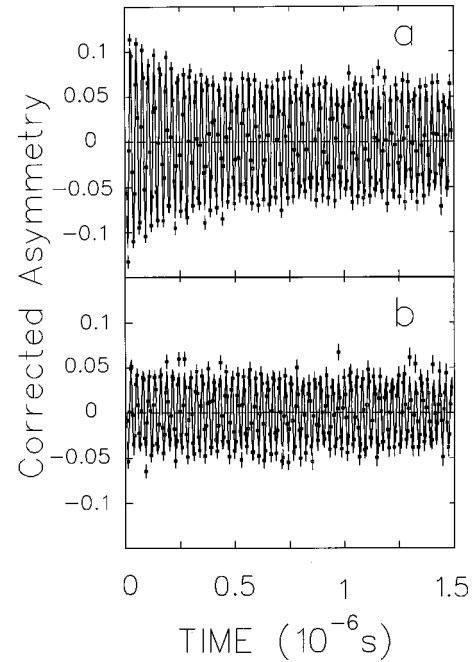


FIG. 2. Diamagnetic signals in solid nitrogen in a transverse magnetic field $H=0.2724$ T in (a) β -N₂ at $T=59$ K and (b) α -N₂ at $T=29$ K. Note the fast-relaxing component in β -N₂.

α - β transition. The *F* component was undetectable in α -N₂ below about 30 K. Therefore expression (5) for the overall muon asymmetry was modified for temperatures above 30 K to

$$A_B^0 P_z(t) = A_{\text{Mu}} e^{-\lambda_{\text{Mu}} t} \cos(\omega_{\text{Mu}} t + \phi_{\text{Mu}}) + [A_F e^{-\lambda_F t} + A_S e^{-\lambda_S t}] \cos(\omega_{\mu} t + \phi_D), \quad (7)$$

where A_F and A_S are the fast-relaxing and slow-relaxing diamagnetic asymmetries and λ_F and λ_S are the corresponding relaxation rates. For temperatures below 30 K the data were fitted to Eq. (5). Figure 2 shows typical diamagnetic signals in solid β -N₂ (a) and α -N₂ below 30 K (b) in a transverse magnetic field $H=0.2724$ T. The *F* component is clearly seen in β -N₂.

The fast-relaxing diamagnetic component was first observed in comparatively low magnetic fields (below 10 mT) in our previous measurements.²⁵ However, experiments in low magnetic field do not allow precise measurements of the amplitude and relaxation rate of the *F* component. Moreover, the low value of the *F* component’s amplitude at some temperatures (around the α - β transition) makes it impossible to distinguish the *F* component from the *S* component in low magnetic field, as the relaxation rate of the *F* component is then higher than its precession frequency. In high magnetic field where the fast-relaxing component was observable for at least ten full oscillation periods, it was possible to unambiguously determine all the parameters of the *F* and *S* components.

The amplitudes of all three components — muonium, slow-relaxing diamagnetic, and fast-relaxing diamagnetic — show peculiar temperature dependences. Figure 3(a) displays the temperature dependences of the muonium and slow-relaxing diamagnetic amplitudes in s -N₂. Most prominent is the strong nonmonotonic variation of both amplitudes, with a

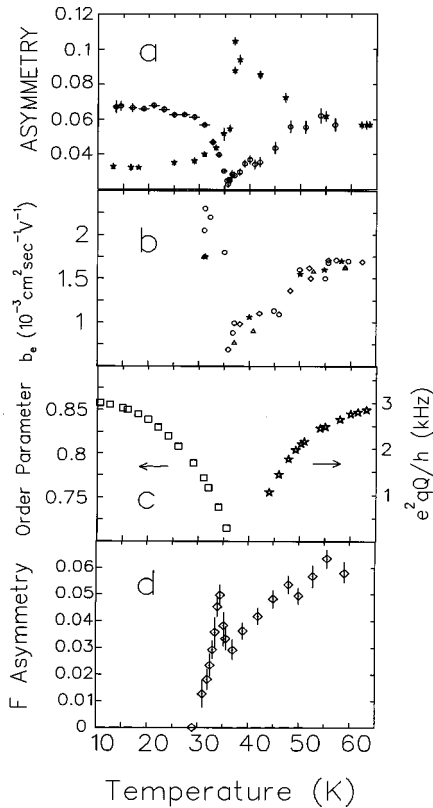


FIG. 3. (a) Temperature dependences of the muonium (circles) and slow-relaxing diamagnetic (stars) amplitudes in solid nitrogen. (b) Temperature dependence of the electron drift mobility in s - N_2 measured by a time-of-flight technique (Ref. 52). (c) Temperature dependences of the orientational order parameter in α - N_2 (Ref. 55) (left) and nuclear quadrupole coupling constant in β - N_2 (right) (Ref. 56). (d) Temperature dependence of the fast-relaxing diamagnetic amplitude in s - N_2 .

minimum in the Mu asymmetry and a corresponding maximum in the S asymmetry around the α - β transition. Such strong temperature dependences are unlikely to be explained by any mechanism taking place at epithermal energies during μ^+ thermalization (the so-called “prompt” muonium formation process). Furthermore, the slow-relaxing diamagnetic signal in solid nitrogen has been determined to be a manifestation of the formation of a $N_2\mu^+$ molecular ion.⁵⁰ This linear ion has about the same binding energy — approximately 5 eV — as an analogous N_2H^+ ion.⁵¹ The polarization of neighboring nitrogen molecules by the charge of the $N_2\mu^+$ ion adds about 1 eV to the binding energy due to the interaction between the ion and the lattice. Therefore one may expect the $N_2\mu^+$ ion to form every time a muon thermalizes as a bare μ^+ , and any variation of the diamagnetic signal amplitude with temperature (for $T < 100$ K) must have some other cause.

The strong anticorrelation between the temperature dependences of A_{Mu} and A_S suggests competition between Mu and diamagnetic species formation. Since the Mu atom ionization potential of 13.54 eV considerably exceeds that of the $N_2\mu^+$ ion in solid nitrogen, the spontaneous formation of the ion from thermal muonium is impossible. The maximum in A_S is therefore not directly due to an increased probability of diamagnetic ion formation, but rather indirectly due to a *de-*

creased probability of Mu atom formation, which has been unambiguously shown to be at least partially due to convergence of the positive muon and an electron liberated in its ionization track in solid nitrogen.²⁵ Such “delayed” Mu formation is expected to depend strongly on the charges’ mobilities. The $N_2\mu^+$ ion is known to be immobile in the nitrogen lattice⁵⁰ (like any other positive species⁵²). Therefore delayed Mu formation in solid nitrogen is believed to be due to electron transport through the lattice to an unmoving $N_2\mu^+$ ion, with the Mu formation time determined by the electron mobility. This picture is further corroborated by the temperature dependence of the electron drift mobility in solid nitrogen, shown in Fig. 3(b), which was measured by a time-of-flight (TOF) technique.⁵² It is remarkable that the $b_e(T)$ dependence so closely resembles that of A_{Mu} in β - N_2 and in α - N_2 at temperatures higher than 30 K; the Mu formation probability even changes in the same proportions as the electron mobility.

The results of TOF measurements in solid nitrogen (as well as in some other diatomic solids) showed that the electron drift mobility lies between 10^{-3} and 10^{-2} $cm^2 s^{-1} V^{-1}$. Experiments in solid CO and O₂ (Ref. 52) and solid H₂ (Refs. 53 and 54) revealed electron mobilities of less than 10^{-2} $cm^2 s^{-1} V^{-1}$. Such low b_e values suggest that the electron is *localized* in these diatomic solids. The electron interaction with orientational degrees of freedom of N₂ molecules has been proposed as a possible mechanism for electron localization in solid nitrogen.⁵² The analysis of our experiments strongly supports this assumption (see below). Interaction with the molecular librational modes determines the electron transport and, consequently, delayed muonium formation in solid nitrogen.

Figure 3(c) shows the temperature dependence of the molecular orientational order parameter in α -nitrogen⁵⁵ derived from nuclear quadrupole resonance (NQR) frequency measurements.⁵⁶ Up to about 20 K the NQR data fit fairly well to Bayer theory,⁵⁷ which invokes small-angle librations to describe molecular dynamics. However, above about 25 K the NQR measurements deviate markedly from the theoretical curve, revealing an unusually strong temperature dependence.⁵⁶ It should be noted that the specific heat⁵⁸ and thermal expansion⁵⁹ in solid N₂ also show anomalies above about 25 K, as do the spin-spin relaxation time and NQR linewidth.⁵⁶

All these anomalies could be understood only by invoking large amplitude motions. At low temperatures α -N₂ exhibits long-range orientational order of the molecules due to quadrupole-quadrupole interactions with zero-point motion superposed. As the temperature is raised, librational waves are excited and increasingly disrupt the ordering. At about 25 K, however, the average lifetime of librational states becomes comparable to the librational period and shorter at higher temperatures.^{56,55} This implies that the librational states are no longer well defined and the lattice is in a critical state of librational disorder. The Raman spectroscopy data⁶⁰ and neutron diffraction measurements⁶¹ also show considerable softening of the librational modes above about 25 K, which has been discussed in terms of large amplitude molecular orientational motion.⁵⁵

Figure 3(c) also shows the temperature dependence of the nuclear quadrupole coupling constant in β nitrogen.⁵⁶ The

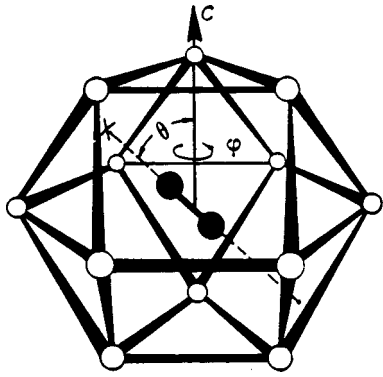


FIG. 4. Orientational structure of β -N₂. Here $\Theta \approx 55^\circ$ is the angle between the long molecular axes and the hexagonal \hat{c} -axis of the crystal. Molecules rotate in the direction denoted by the angle ϕ .

quadrupole coupling constant in β -N₂ is reduced by more than three orders of magnitude with respect to that in α -N₂ by motional averaging. This observation unambiguously demonstrates both that the N₂ molecules reorient in a time shorter than the reciprocal of the static quadrupole resonance frequency (about 10^7 s^{-1}) and that the reorientation is not isotropic (because a nonzero coupling remains). In particular, precession of N₂ molecules about the \hat{c} axis could produce a reduction of the quadrupole coupling constant. The nuclear magnetic resonance (NMR) cannot, however, distinguish a classical precession which is superposed by a small wobble of the precession axis around the \hat{c} -axis of the crystal from a situation where molecules change orientation in a time short compared to the reciprocal of the quadrupole resonance frequency by executing random “jumps” among the six-fold minima in the orientational potential (Fig. 4).^{27,55,62} Either way, analysis of the possible molecular motions has revealed that the value of quadrupole coupling constant is proportional to the order parameter of the molecular librations around the \hat{c} -axis in the *hcp* lattice of β -N₂, which therefore may be considered as partially orientationally ordered.

The temperature dependence of the electron mobility and, therefore, of the delayed Mu formation probability (proportional to the Mu asymmetry) in solid nitrogen turns out to follow that of the molecular orientational order parameter. The electron mobility in α -N₂ measured by TOF technique⁵² [Fig. 3(b)] shows a sharp rise below the α - β transition just like the temperature dependence of the orientational order parameter in *s*-N₂. The same temperature behavior is seen in A_{Mu} [Fig. 3(a)]. Below about 25 K where large-angle librations are not excited and the order parameter almost saturates, the Mu asymmetry is also fairly constant with temperature. Unfortunately, TOF experiments were unable to measure electron mobility in α -nitrogen below 30 K. It will be shown below, however, that electron mobility increases by about 5 orders of magnitude⁴² when the temperature is lowered to the region where large amplitude molecular librations are no longer excited. In β -nitrogen below about 40 K the NMR doublet splitting was too small to be resolved⁵⁶ and, therefore, there is no information on the characteristic times of the molecular reorientations. However, above this temperature the quadrupole resonance frequency [proportional to the order parameter, see Fig. 3(c)] displays the same

temperature dependence as both the electron mobility [Fig. 3(b)] and the Mu asymmetry [Fig. 3(a)]. We conclude that the electron mobility in solid nitrogen (and thus the Mu formation probability) is determined by molecular librations. The slower the molecular reorientations the higher the electron mobility.

This conclusion is supported by comparison of molecular orientational order with electron mobility and with Mu and diamagnetic asymmetries in different phases and different diatomic crystals. In liquid nitrogen, where characteristic molecular reorientation times are known to be higher than in β -N₂ just below the triple point,⁶³ the electron mobility is lower than that in β -N₂,⁵² as expected from the arguments above. Accordingly, the diamagnetic asymmetry drops^{24,64} and the Mu asymmetry rises⁶⁴ as the crystal melts. Analogous behavior is observed in solid CO, which is known to be more orientationally disordered than solid nitrogen in the vicinity of the corresponding triple points.⁶² As expected, the electron mobility in *s*-CO is higher and the diamagnetic muon asymmetry is lower^{26,28} than in *s*-N₂ (Ref. 52) just below triple points. Muonium is not observed directly in condensed CO,²⁶ probably due to formation of MuCO· radicals.⁶⁵ However, in solid CO the peculiarity in molecular reorientation behavior⁶⁶ takes place at the same temperature as the peculiarity in the diamagnetic asymmetry.^{26,28} Comparison of solid β -N₂ and solid ortho-H₂ above the characteristic temperature of orientational ordering,^{27,67} which depends strongly on the ortho concentration, leads to the same conclusion. At these temperatures *s*-H₂ could be considered as a completely disordered crystal,^{27,67} while β -N₂ is partially ordered (see above). The electron mobility in solid hydrogen^{53,54} is about 2–3 orders of magnitude lower than that in β -nitrogen⁵² and, accordingly, the Mu asymmetry in *s*-H₂ (Ref. 21) is considerably lower than that in β -N₂.²⁵

Figure 3(d) shows the temperature dependence of the fast-relaxing diamagnetic asymmetry in solid nitrogen. The relaxation rate of the *F* component ($\lambda_F \approx 5 \text{ } \mu\text{s}^{-1}$) is almost temperature independent and about two orders of magnitude higher than that of the *S* component (also temperature independent). It is reasonable to assume, however, that the *F* component is a manifestation of the same species as the *S* component: the N₂ μ^+ ion.²⁹ The relaxation rate of the *S* component ($\lambda_S \approx 0.1 \text{ } \mu\text{s}^{-1}$) has been shown to be due to nuclear dipole interaction of the μ^+ with ¹⁴N nuclei, primarily those inside the N₂ μ^+ ion.²⁹ The two orders of magnitude higher relaxation rate of the fast-relaxing diamagnetic signal cannot be explained by any interaction of the diamagnetic species with nitrogen nuclear moments. This component must be a direct manifestation of delayed muonium formation due to mobile electrons created in the incoming muon ionization track, N₂ $\mu^+ + e^- \rightarrow \text{Mu} + \text{N}_2$, just like the Mu fraction itself but on a much longer time scale. Strong support for this assumption comes from the fact that the temperature dependence of A_F [Fig. 3(d)] above approximately 35 K is the same as that of $A_{\text{Mu}}(T)$ [Fig. 3(a)] and $b_e(T)$ [Fig. 3(b)], having a minimum at $T_{\alpha\beta}$ where electrons in solid nitrogen are known to be least mobile.

Below about 34 K the *F* component vanishes rapidly with decreasing temperature. No *F* component is seen below about 30 K. We cannot tell from this result whether the *F* component (representing *very* delayed Mu formation by

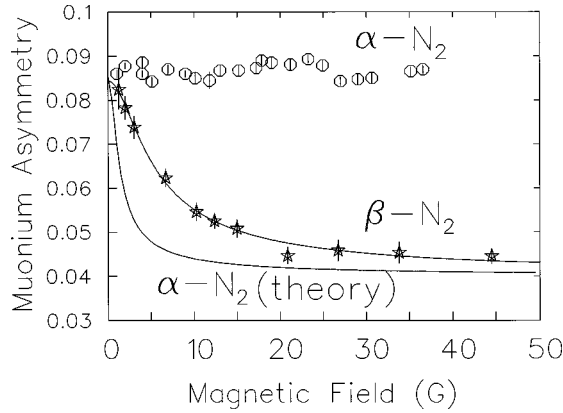


FIG. 5. Magnetic-field dependences of the muonium amplitudes in α -N₂ at $T=20$ K (circles) and in β -N₂ at $T=59$ K (stars). Solid lines represent numerical calculations using values of the electron drift mobility from Ref. 52 in a *localized* electron model.

transport of some *low*-mobility electron species) has been eliminated completely or is still present below 30 K but too short lived to observe with the experimental time resolution.

All these observations confirm that the characteristic times of Mu formation (determined by characteristic electron transport times) are much shorter in α -N₂ below 30 K than in β -N₂. These times can be extracted from the magnetic-field dependence of the muonium asymmetry. Assuming that the delayed muonium formation process is governed by a simple first-order kinetic equation

$$dn_{\text{Mu}}(t) = -dn_{\mu}(t) = \lambda n_{\mu}(t) dt, \quad (8)$$

where λ is the characteristic formation rate, the muonium amplitude has been shown³² to be

$$A_{\text{Mu}} \sim \frac{\lambda}{\sqrt{\lambda^2 + \omega_{\text{Mu}}^2}}. \quad (9)$$

Expression (8) holds true for a constant spatial and time distribution of the e^- with respect to the μ^+ , which is obviously not the case here; nevertheless, Eq. (9) gives a reasonable estimate for the parameter λ . This parameter determines the average transport time $\tau \equiv \lambda^{-1}$ it takes the electron to reach the muon. Equation (9) clearly reflects the phenomenon of delayed Mu formation: different Mu atoms are formed at different times so that phase coherence among precessing Mu atoms is lost. The higher the magnetic field, the stronger the effect of dephasing and the greater the reduction of the Mu asymmetry. Of course, this applies only for delayed Mu formation processes; the prompt Mu asymmetry is essentially magnetic field independent. At high enough magnetic fields, therefore, only the prompt Mu asymmetry remains; this feature can be used to distinguish between the prompt and delayed Mu fractions.

Figure 5 shows the magnetic field dependence of the muonium asymmetry in β -N₂ at $T=59$ K (stars) and in α -N₂ at $T=20$ K (circles). The solid line drawn through the experimental points in β -nitrogen represents a fit to Eq. (10), which takes into account a field-independent prompt muo-

onium asymmetry A_{Mu_p} as well as a delayed muonium asymmetry whose maximum value at low magnetic field is $A_{\text{Mu}_d}(H \rightarrow 0)$:

$$A_{\text{Mu}} = A_{\text{Mu}_p} + A_{\text{Mu}_d}(H \rightarrow 0) \frac{\lambda}{\sqrt{\lambda^2 + \omega_{\text{Mu}}^2}}. \quad (10)$$

The three independent parameters of the fit were $A_{\text{Mu}_p} = 0.041(1)$, $A_{\text{Mu}_d}(H \rightarrow 0) = 0.044(1)$, and $\lambda_{\beta} = 3.2(2) \times 10^7 \text{ s}^{-1}$; i.e., the muonium formation time $\tau_{\beta} = 0.31(2) \times 10^{-7} \text{ s}$. This value is comparable to the delayed Mu formation time in liquid nitrogen, which was determined²⁵ to be approximately $0.4 \times 10^{-7} \text{ s}$.

The characteristic Mu formation time in β -N₂ is almost an order of magnitude shorter than the decay time of the fast relaxing diamagnetic component ($\lambda_{\text{F}}^{-1} \approx 2 \times 10^{-7} \text{ s}$). This may suggest that two different species of radiolysis electrons with mobilities differing by an order of magnitude are formed in the muon's ionization track with roughly the same spatial distribution. (If the F component simply represented electrons liberated further away from the muon's final resting place, they would be much more easily affected by weak electric fields, which is not the case; as shown below, the E -field dependence of the F component is consistent with that of the observable Mu signal.) On the other hand, different time scales of Mu formation and F component may be explained by peculiarities of the spatial distribution of electrons with respect to the μ^+ .

A similar phenomenon (several components of delayed Mu formation with very different characteristic formation times) was observed in superfluid ⁴He,²² where it was attributed to formation of different μ^+ -He clusters. That explanation assumed that μ^+ transport depends on the inner structure of the cluster. It is well established, however, that transport of a heavy enough positive charge (like the positive muon) is determined by its effective mass, which in liquid helium amounts to about 100 times the ⁴He mass [see, for example, Ref. 68]. The mobility of a positive muon in liquid He should therefore be independent of the cluster's structure.

In α -nitrogen the muonium asymmetry is independent of the magnetic field, which means that $\lambda_{\alpha} \gg \omega_{\text{Mu}}$. This inequality allows one to set an upper limit for characteristic Mu formation time in α -N₂: $\tau_{\alpha} \leq 10^{-9} \text{ s}$. Unfortunately, the finite time resolution of the μ SR spectrometer ($\delta t \sim 10^{-9} \text{ s}$) set an upper limit on the transverse magnetic field used in experiment. If the period of the muonium precession in magnetic field H becomes comparable to δt , Mu asymmetry is lost according to Ref. 69,

$$A = A_0 \exp \left[\left(-\frac{1}{4} \omega_{\text{Mu}} \delta t \right)^2 / \ln 2 \right], \quad (11)$$

where A_0 is the Mu asymmetry in infinitesimal transverse field, $\omega_{\text{Mu}} = \gamma_{\text{Mu}} H$, and $\gamma_{\text{Mu}}/2\pi = 1.394 \text{ MHz/G}$ is the Mu gyromagnetic ratio.³ The reduction of the Mu asymmetry according to Eq. (11) has nothing to do with delayed Mu formation and reflects only an apparatus effect due to finite time resolution. Our experiment in α -N₂ revealed A_{Mu} reduction in transverse magnetic fields higher than 5 mT, according to Eq. (11). A simple estimate shows that in this

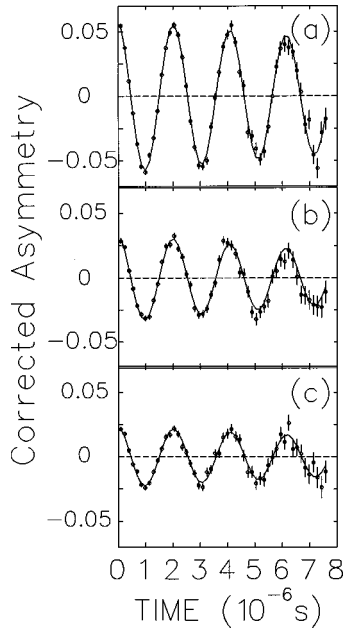


FIG. 6. Diamagnetic precession signals in α -N₂ at $T=20$ K in a transverse magnetic field of 3.5 mT at several electric fields E (a: $E=+7.54$ kV/cm; b: $E=0$; c: $E=-2$ kV/cm).

magnetic field $\omega_{\text{Mu}} \sim \delta t$. Therefore, magnetic-field dependences were measured in $H < 5$ mT. Nevertheless, our results show clearly that the characteristic Mu formation time in α -N₂ is much shorter than that in β -N₂.

Experiments in external electric field show that characteristic muon-electron distances also differ in the α and β phases of solid nitrogen. Figure 6 shows typical diamagnetic precession signals at three different electric fields in α -N₂. A positive sign for E corresponds to the electric field applied parallel to the initial μ^+ momentum direction; if the muon thermalizes *downstream* of the last radiolysis electron it liberates, then a positive E will pull the μ^+ and e^- apart, giving rise to an increased diamagnetic amplitude A_D . Negative E denotes the situation where the electric field is antiparallel to the initial μ^+ momentum.

Figure 7 shows time spectra of the combined (fast and slow) diamagnetic signal for different electric fields in a ro-

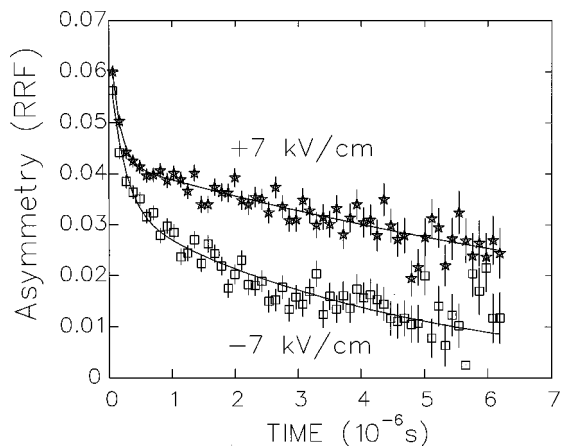


FIG. 7. Diamagnetic precession signals in β -N₂ at $T=59$ K in the rotating reference frame at the muon Larmor frequency for two different electric fields.

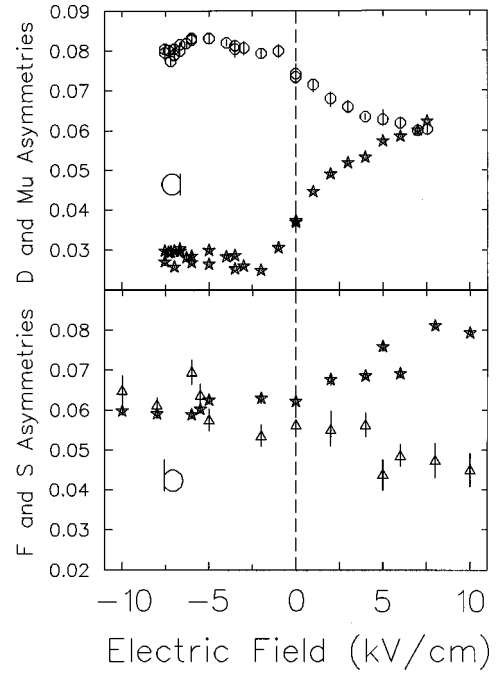


FIG. 8. Electric field dependences of (a) Mu (circles) and slow-relaxing diamagnetic (stars) amplitudes in α -N₂ at $T=20$ K and (b) slow-relaxing (stars) and fast-relaxing (triangles) diamagnetic amplitudes in β -N₂ at $T=59$ K.

tating reference frame⁷⁰ (RRF) at the μ^+ Larmor frequency; this method has been used to remove the oscillatory precession signal and present only the envelope of the signal amplitude, the better to display the two (F and S) components. Figures 6 and 7 show clearly that a sufficiently strong external electric field changes the experimental spectra dramatically.

Figure 8(a) presents the electric field dependences of Mu and diamagnetic amplitudes in α -N₂ at $T=20$ K. Note that A_{Mu} decreases by about half as much as A_D increases. This is because the amplitude of the Mu signal represents only half of the muonium ensemble; the other half oscillates between singlet and triplet states at a frequency that is too high to be observed in our apparatus.³

Figure 8(b) shows the electric field dependences of the fast and slow diamagnetic amplitudes in β -N₂ at $T=59$ K. It is obvious that the electric-field dependence of the slow diamagnetic component is much weaker in β -N₂ than in α -N₂, which probably reflects a shorter μ^+e^- distance in β -N₂ than in α -N₂. The muonium component is much smaller in β -N₂ and does not show a noticeable variation with electric field.

As intimated earlier, the E dependences shown in Figs. 8(a) and 8(b) reflect a strong anisotropy in the spatial distribution of free electrons relative to the stopping position of the muon in solid nitrogen: muons are thermalized *downstream* (i.e., in the direction of the initial muon momentum) from the last radiolysis electrons of the muon's ionization track.

The Coulomb field of the muon at a distance r is

$$E_{\mu} = \frac{e}{\epsilon r^2}, \quad (12)$$

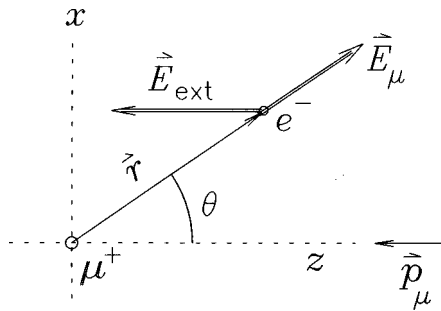


FIG. 9. Sketch showing an arbitrary position of the last radiolysis electron relative to the muon's stopping location. The original muon beam momentum is in the $-\hat{z}$ direction defining a positive sense of the applied electric field E_{ext} .

where e is the elementary charge and $\epsilon = 1.45$ is the dielectric constant of $s\text{-N}_2$. Thus if the muon is a distance $R_{e\mu}$ directly downstream of the last radiolysis electron and a positive external electric field E_{ext} is applied in the $-\hat{z}$ direction (from the electron to the muon), then E_{ext} will pull the electron away from the muon if $R_{e\mu} > \sqrt{e/\epsilon E_{\text{ext}}}$. For example, $E_{\text{ext}} = +5$ kV/cm will overcome the muon's attraction for any electrons at distances ≥ 45 nm or 450 \AA in solid nitrogen. Since the E -dependence shown in Fig. 8(a) seems to be saturating in the neighborhood of $E_{\text{crit}} \sim 5$ kV/cm, we conclude that $\langle R_{e\mu} \rangle = R_\alpha \approx 50$ nm is a typical initial μ^+e^- separation in $\alpha\text{-N}_2$. This is of course only a crude characterization of the spatial distribution, but since our estimate depends on E_{crit} only as its square root, it is probably not too far off.

The absence of any detectable electric field dependence of the muonium asymmetry and the rather weak electric field dependences of the diamagnetic asymmetries make it difficult to determine the characteristic μ^+e^- distance in $\beta\text{-N}_2$. However, a rough estimate can be obtained from comparison of the slopes of the E dependences of the corresponding diamagnetic asymmetries in the two phases, assuming that the net amplitude change would be the same as $E \rightarrow \infty$. This method indicates that $\langle R_{e\mu} \rangle$ is at least a factor of 2 shorter in $\beta\text{-N}_2$ than in $\alpha\text{-N}_2$. The different characteristic muon-electron distances in the α and β phases probably reflect qualitatively different μ^+ thermalization mechanisms in these two phases of solid nitrogen (see below). In liquid nitrogen $\langle R_{e\mu} \rangle$ was estimated to be $R_l \approx 30$ nm,²⁵ comparable to that in $\beta\text{-N}_2$.

In general the electron's initial position will be displaced laterally (in the \hat{x} direction) as shown in Fig. 9. In that case the net force on the electron will be given by

$$\vec{F}_e = \hat{z}e \left[E_{\text{ext}} - \left(\frac{e}{\epsilon r^2} \right) \cos \theta \right] + \hat{x}e \left(\frac{e}{\epsilon r^2} \right) \sin \theta. \quad (13)$$

If the mean free path of an electron is short, it will simply follow electric field lines in "viscous flow" trajectories like those pictured in Fig. 10: wherever on a given trajectory an electron may start, it will follow it the rest of the way to either be captured by the μ^+ or be pulled free by the external field. There is clearly a "boundary" trajectory [in the case shown, it starts at approximately $(x = 170 \text{ nm}, z = 0)$] that encloses the region within which the electron will always be

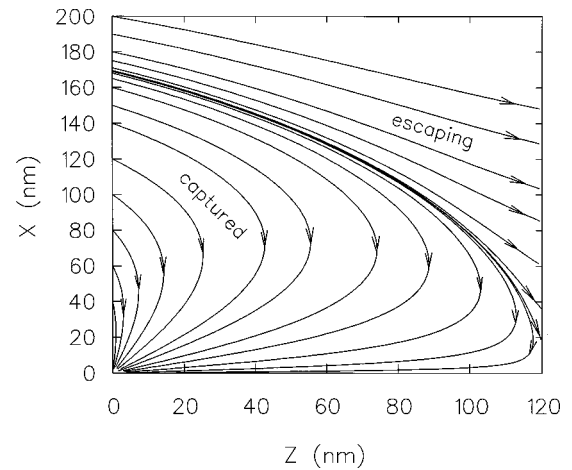


FIG. 10. Trajectories of electrons moving in a viscous flow approximation under the combined influence of an applied electric field of +1 kV/cm and the muon's Coulomb field, assuming a dielectric constant of unity. Note that there is a well defined boundary between the region where the electron eventually escapes and that within which it is eventually captured by the muon.

captured eventually. These "capture boundaries" are displayed in Fig. 11 for a variety of electric fields, assuming $\epsilon = 1$. In each case the actual e^- capture region is a three-dimensional cylindrical solid formed by revolution of the boundary curve about the z axis. If one takes only the finite region enclosed by this surface and the condition $z > 0$, it is not difficult to show that its volume is proportional to $E_{\text{ext}}^{-3/2}$. Of course, once this volume encloses the entire spatial distribution of initial e^- positions relative to the μ^+ , the probability of delayed Mu formation saturates at 100%; so the observed E dependence reflects the overlap between the e^- spatial distribution and the e^- capture region at each electric field.

How can one estimate the average Mu formation time? For this calculation it is best to let $E_{\text{ext}} = 0$ and simply follow the electron back to the muon. In low electric fields ($E \ll u/b_e$, where u is the sound velocity) the electron mobility is independent of electric field and the electron velocity can be expressed as

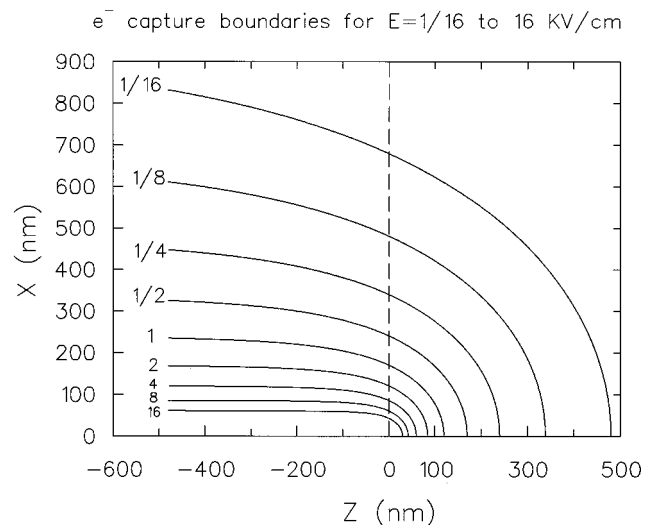


FIG. 11. Loci of e^- capture boundaries for various positive electric fields assuming $\epsilon = 1$.

$$v = b_e E. \quad (14)$$

Integration of Eq. (14) with $E \equiv E_\mu$ from Eq. (12) gives an expression for the Mu formation time,

$$\tau = \lambda^{-1} = \frac{\epsilon}{3eb_e} R^3, \quad (15)$$

where R is the initial distance between the μ^+ and the e^- . Of course, at short distances, where E_μ is large, the electron mobility is certainly no longer constant. However, it can be argued that Eq. (15) is still a good approximation because the time spent traversing the last few nm is a very small fraction of the total recombination time, which is mostly determined by slow motion at large distances. Expressions (9) and (15) allow one to extract the electron mobility b_e from the magnetic field dependence of A_{Mu} , provided the typical value of R is known from the electric field dependence of A_{D} and A_{Mu} .

In fact, this provides the basis of a new technique for studying electron transport in matter.⁴² The electron mobility b_e in a crystal can be extracted provided the muon-electron distance and the characteristic Mu formation time can both be measured for the delayed Mu formation process. This technique has several obvious advantages over the widely used conventional time-of-flight technique (see, for example, Refs. 52, 71, and 72). The latter is based on measurements of the charges' drift times between two electrodes separated by known distance in the material under study. Such measurements of electron drift mobility by TOF techniques have an intrinsic drawback because of the large spacing between the electrodes⁵² (typically on the order of 10^{-2} cm). Such a *macroscopic* characteristic length makes TOF techniques very susceptible to crystalline defects such as impurities, crystal strains, and even crystal cracks (see below).

Evaluation of the electron mobility in $\beta\text{-N}_2$ from Eqs. (9) and (15) with a characteristic $\mu^+ - e^-$ distance $R_\beta = 25$ nm gives $b_e \approx 10^{-3} \text{ cm}^2 \text{ s}^{-1} \text{ V}^{-1}$, which is approximately the same value determined by TOF techniques.⁵² Thus, our experiments confirm that free electrons are *localized* in β -nitrogen.

In order to explain the *localization* of excess charge carriers in diatomic solids, Loveland, Comber, and Spear⁵² used a small-polaron theory⁷³ that describes electron localization as the result of electron interaction with excitations of the medium. This theory treats electron transport as a phonon-assisted hopping process. An attempt to fit experimental results in $\beta\text{-N}_2$ to nonadiabatic small-polaron theory revealed a rather low value of the characteristic energy involved — approximately 50–100 K. This was quite surprising, as one would expect intramolecular phonon modes with an energy almost two orders of magnitude higher to dominate.⁷⁴ This low value of the characteristic energy is, however, consistent with the rotational (librational) modes in a diatomic crystal. Analysis of heat capacity measurements at constant volume⁷⁵ revealed that the contribution of the rotational degrees of freedom of N_2 molecules corresponds to almost free molecular precession accompanied by librations of the precession axis. The characteristic energy of the molecular librations was determined to be $70(2)$ K.²⁷ This value was confirmed in Raman spectroscopy,⁷⁶ infrared absorption,⁷⁷ and inelastic neutron scattering⁶¹ in solid nitrogen. The librational modes

in solid oxygen have almost the same characteristic energy,⁷⁸ while in solid hydrogen the librational modes were found to have somewhat lower energies.²⁷

A possible mechanism for electron localization in $\beta\text{-N}_2$ due to interaction with *optical* phonon modes (whose energies are the same order of magnitude as those of librational modes) can be ruled out because such phonon modes are known only for α -nitrogen⁷⁹ where electrons have been shown to be *delocalized*⁴² (see below). However, electron localization due to interaction with *acoustic* phonon modes near the zone boundary cannot be excluded *a priori*. Unfortunately, as far as the authors know there is no completely self-consistent description of the orientational dynamics in diatomic solids in general or solid nitrogen in particular. The main difficulty is the large inharmonicity of librational motion, even at temperatures well below the temperature of orientational ordering of the crystal. This circumstance, along with the fact that molecules also participate in vibrational dynamics (of their centers of mass), makes the evaluation of lattice dynamics in molecular crystals extremely complicated. Indeed, strong libron-phonon coupling is known to take place in all diatomic molecular crystals.²⁷ Nevertheless, a natural simplification involving independent evaluation of the translational and librational subsystems in diatomic solids gives a qualitatively correct description of the dynamical lattice properties.²⁷

Numerical calculations of the magnetic-field dependence of the muonium asymmetry in $\alpha\text{-N}_2$ according to Eqs. (9) and (15), using the characteristic $\mu^+ - e^-$ distance $R_\alpha = 50$ nm determined from the electric-field dependence [Fig. 8(a)] and the electron mobility b_e extracted from TOF measurements at 30 K,⁵² are shown by the theoretical curve in Fig. 5. In contrast to the good agreement between TOF and μSR measurements in $\beta\text{-N}_2$, a comparison between the experimental and calculated curves in $\alpha\text{-N}_2$ suggests that the Mu formation time is much shorter (and therefore the electron mobility is much higher) by several orders of magnitude than expected from TOF measurements. This has a natural explanation in terms of the mechanical properties of solid nitrogen (see below).

It is known²⁷ that solid N_2 undergoes a huge change in volume at the α - β transition. According to results obtained by different techniques^{80,75,81} this change amounts to about 1% of the crystal volume. Such a big volume change inevitably leads to the creation of strong thermal strains and crystal cracks. Direct optical examination in reflected light confirms the tendency of $\alpha\text{-N}_2$ to develop cracks at the α - β transition.²⁷

The signal height drop observed in the TOF experiments at the α - β transition temperature was attributed to a decrease in the efficiency of generation of free electrons. The latter could have resulted from trapping centers introduced by the large thermal strains at the α - β transition. It should be noted that the distortion of the external electric field by polarization of the medium around trapped electrons (due to thermal strains, cracks, and/or impurities) requires special procedures for executing the space-charge neutralization pulses preceding each electron transit in TOF experiments. There seems no reason to expect that this effect was eliminated completely.⁵² Thus the large thermal strains and cracking of the crystal at the α - β transition were probably the reasons

for the absence of any data on electron mobility below 30 K measured by the TOF technique⁵² in solid nitrogen. We claim that the μ SR technique, which involves *microscopic* characteristic distances (approximately 10–100 nm), avoids the difficulties of the *macroscopic* TOF technique.

The value of the upper limit for the muonium formation time in α -N₂ (see above) allows one to set a lower limit for the electron mobility: $b_e \geq 10^2 \text{ cm}^2 \text{ s}^{-1} \text{ V}^{-1}$ — a value several orders of magnitude higher than that in β -N₂. The high electron mobility in α -N₂ gives us grounds to suggest that the electron transport mechanism in this orientationally ordered phase of solid nitrogen is fundamentally different from that in β -N₂. Probably the *localization* of free electrons *does not occur* in α -N₂.

Electron delocalization was invoked to describe charge transport phenomena in monatomic rare gas solids,^{82,72} which were found to be basically different from those in diatomic solids.⁵² The remarkable transport properties of the rare gas solids, whose electron drift mobilities were measured to be of the same order of magnitude (approximately $10^3 \text{ cm}^2 \text{ s}^{-1} \text{ V}^{-1}$) as those in wide-gap semiconductors, were explained in the framework of the Shockley's theory,⁸³ which suggests that the excess electrons occupy a conduction band. A picture of the free charge carrier as completely delocalized, with the electron-phonon interaction treated as a perturbation, was shown to be a good approximation.⁷² A more general electron transport theory⁸⁴ is based on Shockley's approach while taking into account the structure of the medium containing the electrons. Good agreement with experiment gives one confidence that this description in terms of quasifree band propagation of electrons is valid in rare-gas solids.

The high value of the electron mobility in α -nitrogen leads to a breakdown of the proportionality between v and E [see Eq. (14)] at comparatively moderate electric field $E \gg u/b_e$:⁸³

$$v = (32/3\pi)^{1/4} (b_e E u)^{1/2}. \quad (16)$$

This result is obtained by evaluation of a “hot” electron scattering off crystal excitations. Shockley's approach is based on the assumption that in a weakly scattered electronic system the electric field displaces the electronic energy distribution towards higher energies while it (the electron energy distribution) remains Maxwellian. In low electric fields the rate of energy gain by the electron from the applied field is equal to the electron's rate of energy loss by scattering off lattice excitations, so that Eq. (14) is valid. In a system where “effective” lattice excitations are somehow suppressed (as by the freezing out of the orientational degrees of freedom in α -N₂ due to orientational ordering) this energy loss channel becomes ineffective at high enough electric fields and the electron subsystem is no longer in thermal equilibrium with the lattice, which causes “heating up” of the electron energy distribution and a transition from Eq. (14) to Eq. (16). Such a characteristic transition from a linear dependence (14) to a $v \propto E^{1/2}$ regime has been observed experimentally in a number of insulators and semiconductors, for example in rare gas solids^{82,72} and in n -type Ge.⁸⁵

The qualitative differences between charge transport mechanisms in the different phases of solid nitrogen prob-

ably also affects the slowing down of epithermal muons. For both electrons and muons, the energy loss mechanism in large band gap solids (He, Ne, Ar, Kr, Xe, N₂, etc.) is relatively ineffective when the energetic particle's kinetic energy is less than the band gap. The only possible energy loss channel is then scattering of the particle by crystal excitations (phonons, librions, etc.). Probably energy loss through interactions with orientational degrees of freedom of N₂ molecules is also effective for muons. This channel, however, is suppressed in α -N₂ due to “freezing out” of orientational molecular motion. This is probably why the characteristic $\mu^+ - e^-$ distances are so different in α and β nitrogen where the traditional energy loss channel through scattering off phonons is believed to be the same. This feature could be highly relevant to the development of slow positive muon sources.⁸⁶

In treating the muon and electron as an isolated pair influenced only by their mutual Coulomb attraction and any external field, we have neglected several well-known phenomena that might complicate this picture. The first is the possibility that the electron might diffuse away from the muon through simple thermal motion; this is likely only if the mean thermal energy is comparable to the Coulomb binding energy of the pair at their initial separation — a criterion which defines the Onsager radius,⁸⁷ $R_c = e^2/\epsilon k_B T$, outside which electron transport can be considered as diffusive. Since the characteristic muon-electron distances in s -N₂ turn out to be at least an order of magnitude less than R_c , our picture of the electron “falling into the muon” according to Eqs. (14) and (16) seems to be an adequate description.

We have also neglected the possible role of the positive ion from which the electron was originally stripped. If the electron-ion distance is less than the electron-muon distance, in the absence of an applied electric field the electron will simply return to its origin and recombine with its parent ion — a process known as “geminate” recombination.⁶ However, based on gas-phase studies^{16,20} one would expect a rather different mechanism for the deposition of the final radiolysis electron: near the end of its range, the still epithermal μ^+ makes its last “pickup” of an electron from a nitrogen molecule to form epithermal muonium, leaving behind a positive N₂⁺ ion. The “hot” Mu atom continues slowing down on its way “downstream,” and may either thermalize as muonium (the “prompt” fraction) or lose its electron in a final stripping collision. In this scenario the final radiolysis electron is likely to be much further from its parent N₂⁺ ion than from the terminal N₂ μ^+ ion²⁹ and so geminate recombination is unlikely to play an important role. In any case the effect of geminate recombination upon the E dependence of Mu formation would be subtle except in cases where it prevented Mu formation completely.

V. CONCLUSIONS

The μ SR measurements reported in this paper illuminate the nature of muonium formation in solid nitrogen over the whole temperature range of the solid phase. In both α and β phases of s -N₂ the results are readily explained in terms of a combination of prompt (epithermal) and delayed (thermal) Mu formation, the latter occurring *via* transport of radiolysis electrons through the lattice to static N₂ μ^+ ions.

Application of external electric field reveals a strong anisotropy of the muon-electron spatial distribution. The muon usually thermalizes “downstream” from the last electron liberated in its ionization track. The electric field dependence also provides an estimate of the characteristic $\mu^+ - e^-$ distance $\langle R_{e\mu} \rangle$. In α -N₂, $\langle R_{e\mu} \rangle = R_\alpha \approx 50$ nm, about twice as large as that in β -N₂, $R_\beta \approx 25$ nm. This difference is ascribed to different mechanisms for energy loss to the lattice during muon thermalization: β -N₂ is thought to be better moderator for the energetic μ^+ than α -N₂ due to the additional channel for energy transfer to the orientational subsystem.

These results suggest a technique for electron mobility measurements based on the phenomenon of delayed Mu formation. This technique, being *microscopic* in nature, has advantages over traditional *macroscopic* time-of-flight techniques. Using this new technique, we have found the electron transport mechanism to be fundamentally different in orientationally ordered α -N₂ and orientationally disordered β -N₂. The electron is shown to be *delocalized* in the α phase, where it has a mobility comparable to that in conventional

semiconductors (about $10^2 \text{ cm}^2 \text{ V}^{-1} \text{ s}^{-1}$). Strong electron *localization* in the β phase leads to a reduction of the electron mobility by about of five orders of magnitude. This effect is believed to be due to small polaron formation *via* strong electron coupling with the precessional modes of nitrogen molecules.

ACKNOWLEDGMENTS

This work was supported by the Canadian Institute for Advanced Research, the Natural Sciences and Engineering Research Council of Canada, and the National Research Council of Canada (through TRIUMF). One of us (V.G.S.) was supported by the INTAS Foundation, the Royal Society of the United Kingdom, the Russian Basic Research Foundation, and the NATO Science Program. He also wishes to express his gratitude to Professor S.T. Belyaev and Professor V.P. Martemyanov for constant encouragement and support. We would like to thank C. Ballard and M. Good for technical assistance.

*Present address: Department of Physics, Dalhousie University, Halifax, NS, Canada B3H 3J5.

¹R.L. Garwin, L.M. Lederman, and M. Weinrich, Phys. Rev. **105**, 1415 (1957).

²J.H. Brewer *et al.*, in *Positive Muons and Muonium in Matter*, Muon Physics, Vol. III, edited by V.W. Hughes and C.S. Wu (Academic, New York, 1975), pp. 3–139.

³A. Schenck, *Muon Spin Rotation: Principles and Applications in Solid State Physics* (Adam Hilger, Bristol, 1986); S.F.J. Cox, J. Phys. C **20**, 3187 (1987); J.H. Brewer, in *Muon Spin Rotation/Relaxation/Resonance*, edited by G. Trigg, Encyclopedia of Applied Physics (VCH, New York, 1994), Vol. 11, p. 23.

⁴V.W. Hughes, Annu. Rev. Nucl. Sci. **16**, 445 (1966).

⁵E. Roduner, P.W. Percival, D.G. Fleming, J. Hochmann, and H. Fischer, Chem. Phys. Lett. **57**, 37 (1978).

⁶D.C. Walker, *Muon and Muonium Chemistry* (Cambridge University Press, 1983).

⁷D.G. Fleming *et al.*, Radiochimica Acta **43**, 98 (1988).

⁸D.J. Arseneau, Ph.D. thesis, University of British Columbia, City, 1992.

⁹*Proceedings of the 6th International Conference on Muon Spin Rotation/Relaxation/Resonance*, edited by J.H. Brewer, R.F. Kiefl, and P.W. Percival (J.C. Baltzer AG, Science Publishers, Basel, Switzerland) in *Hyperfine Interactions* **85-87**, 1994.

¹⁰*Proceedings of the 7th International Conference on Muon Spin Rotation/Relaxation/Resonance*, edited by K. Nagamine, R.M. Macrae, R. Kadono, and K. Nishiyama (J.C. Baltzer AG, Science Publishers, Basel, Switzerland); in *Hyperfine Interact.* **104-106**, 1997.

¹¹V.G. Storchak and N.V. Prokof'ev, Rev. Mod. Phys. **70**, 929 (1998).

¹²B.D. Patterson, Rev. Mod. Phys. **60**, 69 (1988).

¹³R.F. Kiefl and T.L. Estle, in *Hydrogen in Semiconductors*, edited by J. Pankove and N.M. Johnson (Academic Press, New York, 1990), p. 547.

¹⁴Y.J. Uemura, A. Keren, K. Kojima, L.P. Le, G.M. Luke, W.D. Wu, Y. Ajiro, T. Asano, Y. Kuriyama, H. Mekata, H. Kikuchi,

and K. Kakurai, Phys. Rev. Lett. **73**, 3306 (1994).

¹⁵K. Kojima, A. Keren, G.M. Luke, B. Nachumi, W.D. Wu, Y.J. Uemura, M. Azuma, and M. Takano, Phys. Rev. Lett. **74**, 2812 (1995).

¹⁶M. Senba, J. Phys. B **21**, 3093 (1988); **22**, 2027 (1989); **23**, 1545 (1990).

¹⁷S.K. Allison, Rev. Mod. Phys. **30**, 1137 (1958).

¹⁸C.J. Oram, J.M. Bailey, P.W. Schmor, C.A. Fry, R.F. Kiefl, J.B. Warren, G.M. Marshall, and A. Olin, Phys. Rev. Lett. **52**, 910 (1984).

¹⁹R.E. Turner and M. Senba, Hyperfine Interact. **17-19**, 697 (1984).

²⁰J.R. Kempton *et al.*, J. Chem. Phys. **94**, 1046 (1991).

²¹J.H. Brewer *et al.*, Hyperfine Interact. **65**, 837 (1990).

²²E. Krasnoperov *et al.*, Phys. Rev. Lett. **69**, 1560 (1992).

²³V. Storchak, J.H. Brewer, W.N. Hardy, S.R. Kreitzman, and G.D. Morris, Hyperfine Interact. **85**, 109 (1994).

²⁴V.G. Grebinnik *et al.*, Pis'ma Zh. Éksp. Teor. Fiz. **51**, 7 (1990) [JETP Lett. **51**, 6 (1990)]; V.G. Grebinnik *et al.*, Fiz. Nizk. Temp. **16**, 1184 (1990) [Sov. J. Low Temp. Phys. **16**, 685 (1990)]; B.F. Kirillov *et al.*, Hyperfine Interact. **65**, 819 (1990).

²⁵V. Storchak, J.H. Brewer, and G.D. Morris, Phys. Lett. A **193**, 199 (1994).

²⁶V. Storchak *et al.*, Pis'ma Zh. Éksp. Teor. Fiz. **52**, 1173 (1990) [JETP Lett. **52**, 581 (1990)].

²⁷*Cryocrystals*, edited by B.I. Verkin and A.F. Prikhotko (Naukova Dumka, Kiev, 1983).

²⁸G.D. Morris *et al.*, Hyperfine Interact. **85**, 1023 (1994).

²⁹V. Storchak *et al.*, Phys. Lett. A **172**, 77 (1992).

³⁰J.H. Brewer, K.M. Crowe, R.F. Johnson, A. Schenck, and R.W. Williams, Phys. Rev. Lett. **27**, 297 (1971).

³¹J.H. Brewer, F.N. Gyax, and D.G. Fleming, Phys. Rev. A **8**, 77 (1973).

³²P.W. Percival, E. Roduner, and H. Fischer, Chem. Phys. **32**, 353 (1978).

³³F.M. Jacobsen, Hyperfine Interact. **32**, 501 (1986).

³⁴O.E. Mogensen and P.W. Percival, Radiat. Phys. Chem. **28**, 85 (1976).

- ³⁵P.W. Percival, J.C. Brodovitch, and K.E. Newman, *Chem. Phys. Lett.* **91**, 1 (1982).
- ³⁶E. Roduner, G.A. Brinkman, and P.W.F. Louwrier, *Chem. Phys.* **88**, 143 (1984).
- ³⁷P.W. Percival *et al.*, *Chem. Phys.* **95**, 321 (1985).
- ³⁸E. Krasnoperov *et al.*, *Hyperfine Interact.* **87**, 1017 (1994).
- ³⁹V. Storchak, J.H. Brewer, and G.D. Morris, *Phys. Rev. Lett.* **76**, 2969 (1996).
- ⁴⁰V.G. Storchak, J.H. Brewer, and S.F.J. Cox, *Hyperfine Interact.* **105**, 189 (1997).
- ⁴¹V.G. Storchak, J.H. Brewer, and D.G. Eschenko, *Appl. Magn. Reson.* **13**, 15 (1997).
- ⁴²V. Storchak, J.H. Brewer, and G.D. Morris, *Phys. Rev. Lett.* **75**, 2384 (1995).
- ⁴³V. Storchak, J.H. Brewer, and G.D. Morris, *Phys. Rev. B* **56**, 55 (1997).
- ⁴⁴L. Jansen and F. de Wette, *Physica (Amsterdam)* **22**, 83 (1955).
- ⁴⁵B.C. Kohin, *J. Chem. Phys.* **33**, 882 (1960).
- ⁴⁶L. Pauling, *Phys. Rev.* **36**, 430 (1930).
- ⁴⁷W.E. Streib, T.H. Jordan, and W.N. Lipscomb, *J. Chem. Phys.* **37**, 2962 (1962).
- ⁴⁸V.A. Slusarev *et al.*, *Phys. Status Solidi* **54**, 745 (1972).
- ⁴⁹T.N. Antsygina *et al.*, *J. Low Temp. Phys.* **56**, 331 (1984).
- ⁵⁰V. Storchak *et al.*, *Chem. Phys. Lett.* **200**, 546 (1992).
- ⁵¹W.P. Kraemer, A. Komornicki, and D.A. Dixon, *Chem. Phys.* **105**, 87 (1986).
- ⁵²R.J. Loveland, P.G. Le Comber, and W.E. Spear, *Phys. Rev. B* **6**, 3121 (1972).
- ⁵³P.G. Le Comber *et al.*, *Solid State Commun.* **18**, 377 (1976).
- ⁵⁴A.A. Levchenko and L.P. Mezhov-Deglin, *Pisima Zh. Éksp. Teor. Fiz.* **48**, 401 (1988) [*JETP Lett.* **48**, 442 (1988)].
- ⁵⁵T.A. Scott, *Phys. Rep.* **27C**, 89 (1976).
- ⁵⁶A.S. DeReggi, P.C. Canepa, and T.A. Scott, *J. Magn. Reson.* **1**, 144 (1969).
- ⁵⁷H. Bayer, *Z. Phys.* **130**, 227 (1951).
- ⁵⁸M.I. Bagatskii *et al.*, *Phys. Status Solidi* **26**, 453 (1968).
- ⁵⁹V.G. Manzhelii, A.M. Tolkachev, and E.I. Voitovich, *Phys. Status Solidi* **13**, 351 (1966).
- ⁶⁰P.M. Mathai and E.J. Allin, *Can. J. Phys.* **49**, 1973 (1971).
- ⁶¹J.K. Kjems and G. Dolling, *Phys. Rev. B* **11**, 1639 (1975).
- ⁶²Yu.A. Freiman, *Sov. J. Low Temp. Phys.* **16**, 955 (1990).
- ⁶³L.M. Ishol, T.A. Scott, and M. Goldblatt, *J. Magn. Reson.* **23**, 313 (1976).
- ⁶⁴J.H. Brewer, G.D. Morris, and V. Storchak (unpublished).
- ⁶⁵S.F.J. Cox *et al.*, *Hyperfine Interact.* **65**, 773 (1990).
- ⁶⁶F. Li *et al.*, *J. Chem. Phys.* **74**, 3120 (1981).
- ⁶⁷I.F. Silvera, *Rev. Mod. Phys.* **52**, 393 (1980).
- ⁶⁸V.B. Shikin, *Usp. Fiz. Nauk*, **121**, 457 (1977) [*Sov. Phys. Usp.* **20**, 226 (1977)].
- ⁶⁹E. Holzschuh, *Phys. Rev. B* **27**, 102 (1983).
- ⁷⁰T.M. Riseman and J.H. Brewer, *Hyperfine Interact.* **65**, 1107 (1990).
- ⁷¹M.H. Shal'nikov, *Zh. Éksp. Teor. Fiz.* **41**, 1059 (1961) [*Sov. Phys. JETP* **14**, 755 (1962)].
- ⁷²W.E. Spear and P.G. Le Comber, in *Electronic Transport Properties, Rare Gas Solids*, edited by M.L. Klein and J.A. Venables (Academic, New York, 1977), p. 1120.
- ⁷³T. Holstein, *Ann. Phys. (Leipzig)* **8**, 343 (1959).
- ⁷⁴W. Seibrand, *J. Chem. Phys.* **41**, 3574 (1964).
- ⁷⁵I.N. Krupskii, A.I. Prokhorov, and A.I. Erenburg, *Fiz. Nizk. Temp.* **1**, 359 (1975) [*Sov. J. Low Temp. Phys.* **1**, 178 (1975)].
- ⁷⁶F.D. Medina and W.B. Daniels, *J. Chem. Phys.* **64**, 150 (1976).
- ⁷⁷U. Buontempo *et al.*, *Phys. Lett.* **A74**, 113 (1979).
- ⁷⁸J.E. Cahill and G.E. Leroi, *J. Chem. Phys.* **51**, 97 (1969).
- ⁷⁹A. Anderson, T.S. Sun, and M.C.A. Donkersloot, *Can. J. Phys.* **48**, 2265 (1970).
- ⁸⁰D.C. Heberlein, E.D. Adams, and T.A. Scott, *J. Low Temp. Phys.* **2**, 449 (1970).
- ⁸¹C.A. Swenson, *J. Chem. Phys.* **23**, 1963 (1955).
- ⁸²L.S. Miller, S. Howe, and W.E. Spear, *Phys. Rev.* **166**, 871 (1968).
- ⁸³W. Shockley, *Bell Syst. Tech. J.* **30**, 900 (1951).
- ⁸⁴M.H. Cohen and J. Lekner, *Phys. Rev.* **158**, 305 (1967).
- ⁸⁵E.J. Ryder and W. Shockley, *Phys. Rev.* **81**, 139 (1951).
- ⁸⁶E. Morenzoni *et al.*, *Phys. Rev. Lett.* **72**, 2793 (1994).
- ⁸⁷L. Onsager, *Phys. Rev.* **54**, 554 (1938).